Journal of Bone Oncology 29 (2021) 100378

Contents lists available at ScienceDirect

Journal of Bone Oncology

journal homepage: www.elsevier.com/locate/jbo

Research Paper

Establishment and characterization of a highly metastatic human osteosarcoma cell line from osteosarcoma lung metastases

Zepei Fan [a,1], Guanyu Huang [a,1], Jupeng Zhao [a,1], Wuguo Li [b], Tiao Lin [a,c], Qiao Su [b], Junqiang Yin [a,c,*], Jingnan Shen [a,c,*]

[a] Department of Musculoskeletal Oncology, the First Affiliated Hospital of Sun Yat-Sen University, Guangzhou, Guangdong, China
[b] Department of Animal Experiment Center, the First Affiliated Hospital of Sun Yat-sen University, Guangzhou, Guangdong, China
[c] Guangdong Provincial Key Laboratory of Orthopedics and Traumatology, the First Affiliated Hospital of Sun Yat-Sen University, Guangzhou, Guangdong, China

ARTICLE INFO

Article history:
Received 25 December 2020
Revised 10 June 2021
Accepted 18 June 2021
Available online 22 June 2021

Keywords:
ZOSL-1
Osteosarcoma
Pulmonary metastasis

ABSTRACT

OS (Osteosarcoma) is the most common malignant tumor in adolescents, and lung metastasis limits its therapeutic outcome. The present study aimed to establish a highly metastatic human OS cell line directly from lung metastases and characterize its biological functions. In this study, epithelioid tumor cells with large nucleo-cytoplasmic ratio and abundant organelles were obtained by the tissue mass adherent and repeated digestion adherent method and named ZOSL-1 cells. ZOSL-1 cells had the potential to proliferate in vitro with a doubling time of 39.28 ± 3.04 h and migrate with or without a matrix. ZOSL-1 cells were tumorigenic *in vivo*, and had the ability to develop lung metastasis after intratibial injection. ZOSL-1 cells expressed the osteogenic-related genes osteocalcin and osteopontin. In addition, the expression of ZOSL-1 in Fas cell surface death receptor (FAS), CD44 molecule (CD44), GNAS complex locus (GNAS), scavenger receptor class B member 1 (SCARB1), C-X-C motif chemokine receptor 4 (CXCR4), cadherin 11 (CDH11), neurofibromin 2 (NF2) and ezrin (EZR) genes may be related to its transfer efficiency. Taken together, these results indicated the high metastatic capability and important biological functions of ZOSL-1 cells. ZOSL-1 establishment provided a relevant model for the study of osteosarcoma lung metastasis.

1. Introduction

OS (Osteosarcoma) originates from mesenchymal malignant proliferation and represents the most common primary malignant bone tumors. It has two peaks, one in the late adolescent and young adult period, and another in or after the 6th decade of life. High fatality rates have been observed due to lung metastasis, which occur in a short period of time [1,2]. With the major surgery combined with chemotherapy in the neoadjuvant chemotherapy treatment, the 5-year survival rate improved to 60% to 70%, but with distant metastasis in patients, such a rate decreased to 20% to 30% [3,4]. Further research to understand the OS mechanism of occurrence and metastasis is of great significance for its treatment.

Cell lines are important in vitro models of disease. Ponten and Saksela established the U2-OS cell line isolated from a 15-year-old girl with a moderately differentiated osteogenic sarcoma [5]. This cell line is widely used for the in vitro study of OS [6–8]. The U2OS/MTX300 cell line was obtained by exposing U2-OS cells in vitro to stepwise increasing methotrexate (MTX) concentrations, which has been widely used in the study of drug resistance mechanisms in OS [9]. The HOS cell line was also established. It was derived from an OS of the distal right femur of a 13-year-old Caucasian girl [10]. Luu *et al.* further modified and established the MNNG/HOS and 143B cell lines [11], which for exploring metastasis of OS. However, most of the current OS cell lines are derived from *in situ* OS lesions, and their metastatic capacity is limited. Zou *et al.* isolated Zos and Zos-M cells from primary tumor and the skip metastasis of an OS patient, and proved that Zos-M had stronger metastasis efficiency in vitro and *in vivo* than Zos [12]. Currently, there were no stable OS cell line was established directly from lung metastasis tissue. Due to the lack of lung metastasis cell lines, researchers were unable to directly study the lung metastasis mechanism of OS cells, which hindered the study of lung metastasis of OS cells.

To directly explore the mechanisms of lung metastasis in OS, we sought to isolate OS cells from lung metastases and establish stable cell lines. Our study is the first report in the world that OS cells

* Corresponding authors at: Department of Musculoskeletal Oncology, the First Affiliated Hospital of Sun Yat-Sen University, Guangzhou 510080, China.
E-mail addresses: yinjunq@mail.sysu.edu.cn (J. Yin), shenjn@mail.sysu.edu.cn (J. Shen).
[1] Zepei Fan, Guanyu Huang and Jupeng Zhao contributed equally to this work.

https://doi.org/10.1016/j.jbo.2021.100378

from human lung metastases were successfully extracted and cultured into cell line. Riggs et al. isolated OS cells directly from the lung metastasis of an 11-year-old female poodle in 1974, named D17 [13]. The cell line has a strong metastasis capacity. The establishment of the D17 cell line provides the feasibility of obtaining lung metastasis cells directly. In our study, we isolated an OS cell line from pulmonary metastasis tissues, using the tissue mass adherent and repeated digestion adherent method, and evaluated its morphology, proliferation and migration in vitro, genetic information, and tumorigenic and metastatic potential *in vivo*.

2. Materials and methods

2.1. Establishment of ZOSL-1 cell line

Tumor cells originated from the left upper tibial OS and pulmonary metastasis of a 12-year-old female patient at the First Affiliated Hospital of Sun Yat-sen University. The subtype of the primary tumor was osteoblastic OS (Supplementary Fig. S1). Informed consent for the experimental use of the specimens was obtained from the patient and her parents. About 1 cm^3 of diseased lung tissue was obtained during the operation, preserved under aseptic conditions, and transported to the laboratory at low temperature.

Under the aseptic condition, the tissue blocks were transferred to a centrifuge tube containing 30 mL of phosphate buffer saline (PBS; Gibco, New York, USA, C10010500BT), washed to remove the blood on the tissue surface. The surrounding connective tissue was removed and the tumor tissue was cut into 1 mm^3 pieces. Tissue blocks were inoculated in a disposable culture dish, and dried at 37 °C for 20 min. Next, 3 mL of fresh medium was added to the culture and changed once every 3 days, until cells around the tissue block emerged. After this, culture medium volume was increased to 10 mL and changed once every 3 days, until cell density around the tissue block reached about 70%. Cells were collected and then adjusted to a plate inoculation density of 10^5/cm^2 for P1. After P1 cells grew to more than 80% confluency, cells were treated with 0.25% trypsin at 37 °C for 3 min to 5 min and incubated in culture dishes for 30 min. Supernatant was removed to continue the adherent cultures. P2 cells growth was continued according to the above passage method, after growing to 80% confluency. After showing local aggregation and cells growth, and the appearance of epithelioid cells, the partial digestion method was used to obtain the cells, and stable tumor cells could be obtained after multiple passages.

2.2. Cell culture and transfection

ZOSL-1 cells were cultured in dulbecco's modified eagle medium (DMEM; Gibco, New York, USA, C11995500BT) supplemented with 10% foetal bovine serum (FBS; Gibco, New York, USA, 10270-106) at 37 °C in a 5% CO_2 incubator. The normal osteoblastic cell line hFOB 1.19 used for comparison was obtained from the American Type Culture Collection (ATCC® CRL-11372™), and were cultured at 34 °C according to instructions from ATCC.

The virus suspension of mCherry were purchased from HanBio (Shanghai, China). ZOSL-1 cells were transfected with mCherry according to manufacturer's instructions. Cells were used for *in vivo* experiments two weeks after expansion.

2.3. Morphological observations

The morphology of the living cells in the culture flasks was observed under an inverted microscope and pictures were taken. In addition, sections were stained with uranyl acetate and lead citrate and examined under a transmission electron microscope.

2.4. Cell growth and clone formation assay

Cell growth was determined using the cell counting kit-8 (CCK-8; Dongren, Shanghai, China, CK04) assay and clone formation assay. ZOSL-1 cells were seeded onto 96-well culture plates at a density of 2000 cells/well. After culturing for 8 h, 10 μL of CCK-8 were added to each well and incubated for 3 h. Formazan was dissolved and optical densities (ODs) were quantified by microplate reader (BioTek, Vermont, USA, 800 TS) at 450 nm. The test was performed for next six days of culture to produce a cell growth curve.

In addition, ZOSL-1 cells were seeded onto 6-well culture plates at a density of 500 cells/well, changing the medium once every 3 days. About 2 weeks later, after the cell mass was visible to the naked eye, cells were fixed with 75% alcohol, and the size and number of clones were observed by 0.5% crystal violet (Leagene, Beijing, China, DZ0054) staining.

2.5. Wound healing and matrigel invasion assay

ZOSL-1 cells were seeded in 6-well plates up to 90% confluency and scratched by a 10 μL lance-gun head perpendicular to the bottom of the plates. After washing and removing the floating cells with PBS and adding serum-free culture medium, the size of the scratches was photographed every 6 h. After 24 h, Image J was used to calculate the scratched area.

The matrix (Corning, New York, USA, 354234) was diluted in the DMEM : matrix ratio of 9:1. Fifty microliters of the matrix were added into a transwell chamber and incubated at 37 °C for 1 h. ZOSL-1 cells (10^5 cells) were then inoculated in the transwell chamber. Two hundred microliters of serum-free medium were used in the upper chamber and 500 μL medium containing 10% FBS was used in the lower chamber. Cells were then incubated for 12 h at 37 °C. Cells in the upper chamber were wiped off with a cotton swab, and cells in the lower chamber were fixed. After crystal violet staining, photographs were obtained.

2.6. Immunofluorescence analysis

ZOSL-1 cells were seeded in cell slides and were used for immunofluorescence detection. Cells were fixed by paraformaldehyde for 20 min and treated by 0.1% triton for 30 min. Then, cells were blocked for 1 h by 10% goat serum, incubated with primary antibodies at 4 °C overnight. These primary antibodies were anti-OP (Proteintech, Chicago, USA, 22952–1-AP), and anti-OC (Proteintech, Chicago, USA, 23418–1-AP). After being washed three times with PBS, cells were incubated for second antibody for 2 h at room temperature in the dark. The second antibody was Alexa Fluor 488 goat anti-rabbit (Abcam, Cambridge, England, ab150077). Hoechst 33,258 (Leagene, Beijing, China, DA0010) staining was performed nucleus.

2.7. Karyotype analysis

The passaged cells in the exponential phase of growth were treated with 0.5 μg/mL colchicine for 2 h. Cells were then harvested and treated with 8 mL hypotonic solution of potassium chloride at 0.075 mol/L at 37 °C for 30 min. Then, added 8 mL stationary liquid which fixed in solution with a volume ratio of acetic acid to methanol of 1:3. After centrifuging, added 8 mL stationary liquid to precipitate and incubated at 37 °C for 20 min and then kept in ice for 10 min. Repeating the previous step, then collected the precipitate and added 500 μL stationary liquid for resuspending. The samples

were stored at 4 °C, and analyzed of karyotype by practical automatic analyzer.

2.8. In vivo tumorigenicity and metastasis

Animal experiments were approved by the Institutional Review Board of the First Affiliated Hospital of Sun Yat-sen University and were performed according to established guidelines for the Use and Care of Laboratory Animals.

For subcutaneous transplantation, 5 nude mice were implanted with subcutaneous tumors and inoculated at left and right sides of the back. ZOSL-1 cells were harvested at 25th passage, and the cell density was adjusted to 2.143×10^7/mL, and 70 μL of cell suspension was inoculated at each place.

For orthotopic transplantation, the 20th passage cells were transfected with mCherry plasmid, and the stable strain was constructed for subsequent experiments. Five NOD-SCID IL-2 receptor gamma null (NSG) mice were implanted with tumors *in situ*, and the left leg was injected. Cell density was adjusted to 7.5×10^7/mL, and 20 μL of cell suspension was inserted to the proximal tibia through the cortex of the anterior tuberosity, using a 30-gauge needle. After 45 days, IVIS Lumina XR Series III Imaging System was used to monitor localization of mCherry-labelled ZOSL-1 cells within animals.

2.9. Whole exome sequencing

The qualified genomic DNA sample of ZOSL-1 cells was randomly fragmented by Covaris technology and the size of the library fragments was mainly distributed between 150 bp and 250 bp. The end repair of DNA fragments was performed and an "A" base was added at the 3′-end of each strand. Adapters were then ligated to both ends of the end repaired/dA tailed DNA fragments for amplification and sequencing. Size-selected DNA fragments were amplified by ligation-mediated polymerase chain reaction (PCR), purified, and hybridized to the exome array for enrichment. The rolling circle amplification (RCA) was performed to produce DNA Nanoballs (DNBs). Each resulting qualified captured library was performed high-throughput sequencing for each captured library. Sequencing-derived raw image files were processed by BGISEQ-500 base-calling. All genomic variations, including SNPs and InDels were detected by the state-of-the-art software, such as Haplotype Caller of GATK (v3.7). After that, the hard-filtering method was applied to get high-confident variant calls.

2.10. Real-time reverse transcriptase polymerase chain reaction

Total RNA was extracted from cells using Total RNA Kit I (Omega Bio-Tek, Georgia, USA, R6834-02), according to products instructions. Extracted RNA was reverse transcribed to cDNA using the PrimeScript™ RT reagent Kit with gDNA Eraser (Takara Bio, Tokyo, Japan, RR047A-5). Transcription levels of the indicated genes and β-actin were detected by RT-PCR on a Real-Time PCR Detection System (Applied Biosystems, Foster City, CA) with TB Green Premix Ex Taq II (Takara Bio, Tokyo, Japan, RR820A), according to manufacturer's protocol. The primer sequences are listed in Supplementary Table S1. Amplification was performed for 40 cycles in a 10 μL reaction volume. Each cycle included 30 s at 95 °C, 5 s at 95 °C, and 34 s at 60 °C.

2.11. Hematoxylin and eosin (H&E) staining

Mouse tumors in back, leg, and lung were fixed in 4% paraformaldehyde, paraffin-embedded, and sliced to 5 μm. The middle position of tissue samples was selected for H&E staining (Servicebio, Wuhan, China, G1005). In brief, slices were baked, dewaxed, rehydrated, hematoxylin stained, eosin stained, dehydrated, and sealed, after which they were observed under the microscope for histological morphology. Tumor structure was then photographed.

2.12. Statistical analysis

Data were analyzed by Student's *t*-test (GraphPad Prism; GraphPad Software, Inc., La Jolla, CA). A value of p values < 0.05 were considered statistically significant. All data were expressed as mean ± standard deviation.

3. Results

3.1. ZOSL-1 cells isolation and morphology

OS lung metastases obtained during surgery were washed with PBS and cut into 1 mm^3 pieces under aseptic conditions. Tissue blocks were then attached to a culture dish for adherent culture. After 2–3 days, cells began to emerge, and after 7 days, cell density around the tissue blocks reached about 70% (Fig. 1a). When transplanted cells were cultured by passaging to the fourth generation, local cells rapidly proliferated and presented polygonal epithelioid cells (Fig. 1b). These cells were obtained by local digestion and repeated adherent methods, which could passage to 50 generations with stable cell morphology (Fig. 1c). Cell cytoplasm was relatively large with multiple nucleoli and abundant organelles, as observed by transmission electron microscopy (Fig. 1d).

3.2. ZOSL-1 cells proliferation characteristics

Proliferation characteristics of ZOSL-1 cells were evaluated by measuring cell growth and clonal formation. CCK-8 results showed a slow cell growth within 5 days. Cells entered the logarithmic

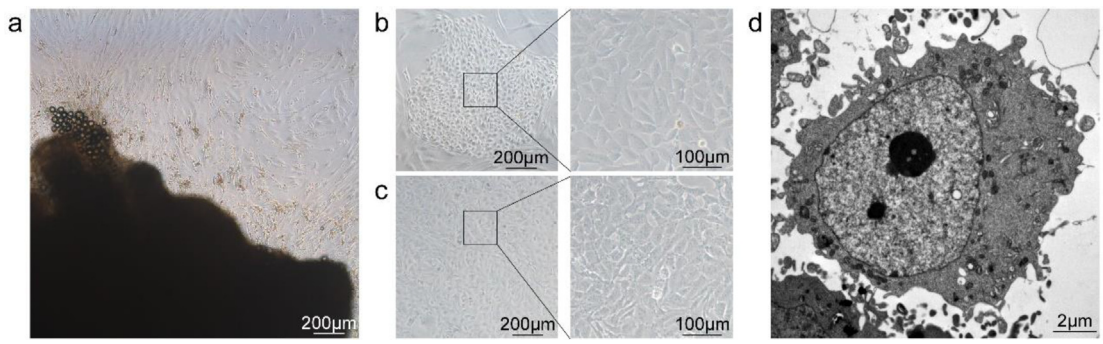

Fig. 1. Acquisition and morphology of ZOSL-1. a: After 7 days of tissue adherence, the density of surrounding cells reached about 70%. b: The 4th generation cells showed local rapid proliferation of polygonal epithelioid cells. c: The 30th generation cells showed polygonal epithelioid cells. d: Transmission electron microscopy of ZOSL-1.

growth period on the 5th to 7th days, with a doubling time of 39.28 ± 3.04 h (Fig. 2a). The result of clone formation showed that ZOSL-1 had significant proliferation potential (Fig. 2b).

3.3. ZOSL-1 cells migration and invasion

Migration and invasion were evaluated on 20th generation ZOSL-1 cells by testing their wound healing effect (Fig. 2c). ZOSL-1 cells migration was evident after 6 h. After 24 h, the cell migration rate was 53.78 ± 0.26% (Fig. 2d). Transwell assay results demonstrated significant invasion activity by ZOSL-1 cells (Fig. 2e).

3.4. Expression of osteoblastic and chondrocytic markers

To determine ZOSL-1 cell lineage, we evaluated the presence of ALP, OC, OP and RUNX2 osteoblast lineage and ACAN, COL Ⅱ, and COL Ⅹ chondrocytic markers by RT-PCR. Results showed that ALP, OC, OP, RUNX2 and COL X expression levels were higher in ZOSL-1 cells, as compared with hFOB 1.19 cells. In contrast, expression levels of ACAN and COL II were lower in ZOSL-1 cells than in hFOB 1.19 cells (Fig. 3a). In addition, we attempted to determine whether ZOSL-1 cells expressed OC and OP at the protein level, and immunofluorescence analysis showed ZOSL-1 cells highly expressed OC and OP (Fig. 3b, c).

3.5. Karyotype analysis of ZOSL-1 cells

The results of karyotype analysis indicated that ZOSL-1 cells carried high chromosomal heterogeneity. ZOSL-1 cells were diploid OS cells and had total of 48 chromosomes. However, chromosomal heterogeneity between different ZOSL-1 cells were significant. (Fig. 4 and Supplementary Fig. S2).

3.6. In vivo tumorigenic and metastatic potential of ZOSL-1 cells

To investigate the tumour-forming and metastatic capability of ZOSL-1 cells *in vivo*, we inoculated ZOSL-1 cells in the subcutaneous and tibial lumen of mice. Results showed that 1.5 million

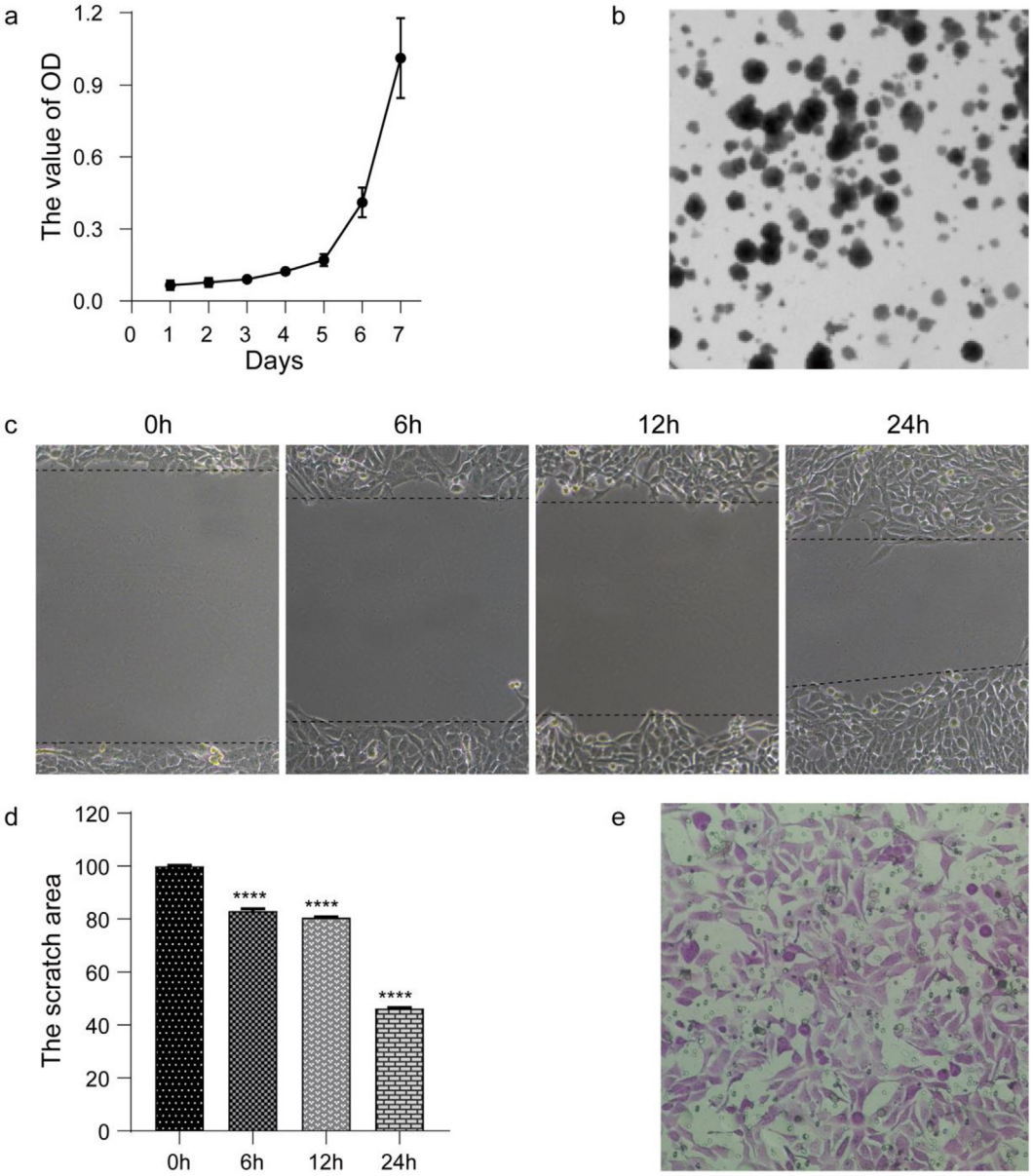

Fig. 2. Proliferation, migration and invasion capability of ZOSL-1. a: The result of CCK-8. b: The result of cloning. c: Scratch detection within 24 h. d: Quantification of scratch results. ****: $p < 0.0001$; ***: $p < 0.001$; **: $p < 0.01$, *: $p < 0.05$. e: The cells migration through the matrigel-coated filter in the transwell chamber.

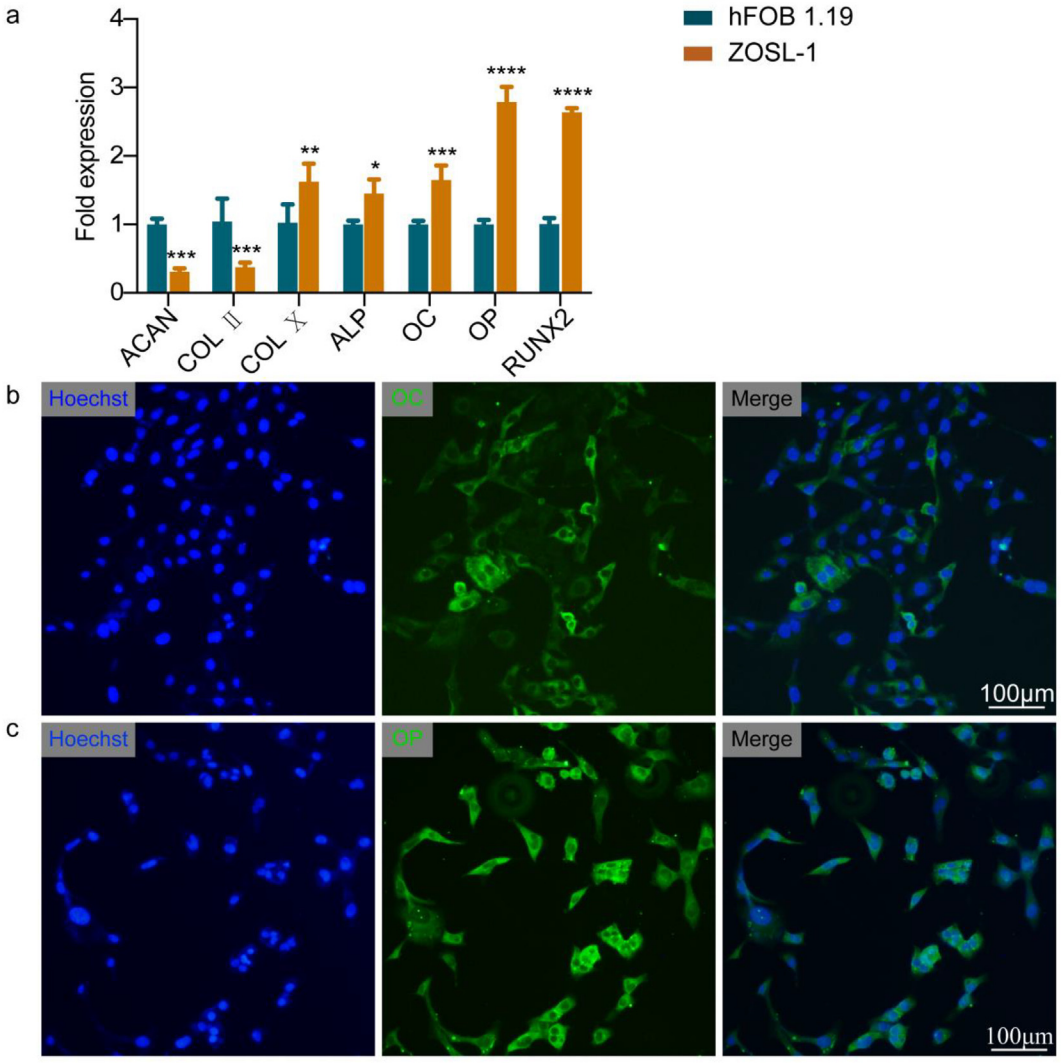

Fig. 3. The expression of osteogenesis and cartilage markers of ZOSL-1 cells. a: RT-PCR to detect expression of ACAN, COL Ⅱ, COL Ⅹ, ALP, OC, OP and RUNX2. ****: $p < 0.0001$; ***: $p < 0.001$; **: $p < 0.01$, *: $p < 0.05$. b: Immunofluorescence was used to detect the expression of OC in ZOSL-1. c: Immunofluorescence was used to detect the expression of OP in ZOSL-1.

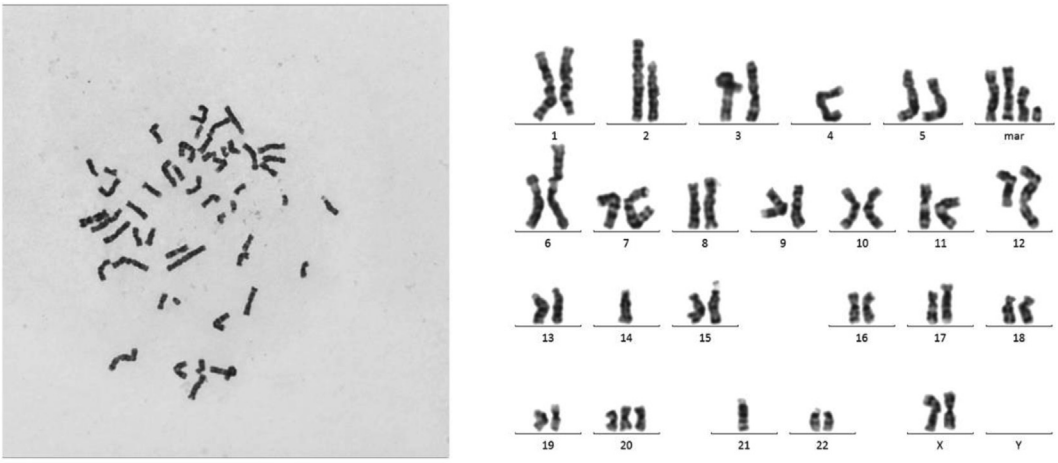

Fig. 4. Karyotype analysis of the 20th generation ZOSL-1 cell. Karyotype: 48,X(1)t(X;9;11)(q24;q22;q24.3);(2)t(1;7)(q25;q32);(3)t(2;6)(p13;q25);(4)-4;(5)-14;(6)der(17)ins(17;?)(q21::?);(7) + 20;(8)der(21)t(1;21)(q25;q22);(9)-21;(10) + 4mar.

cells were inoculated subcutaneously in nude mice, and tumor formation was observed 2 months later, showing 100% tumorigenicity. H&E staining showed dense tumor structure with partial necrosis. The nucleus was large and presented osteoid tissue morphology (Fig. 5a, b).

To further explore the lung metastasis potential of these cells *in vivo*, we transfected cell with red fluorescence, after which cells were injected in the tibial lumen. After 45 days, we performed *in vivo* imaging detection. It was observed that ZOSL-1 produced tumors *in situ* and lung metastasis (Fig. 5c), with 100% tumor formation and lung metastasis rates. Lung tissue was obtained for H&E detection, the formation of lung masses and alveolar deformation were evidenced by squeezing. H&E showed that the histological morphology was similar to the tumor *in situ* (Fig. 5d, e). These results suggest that ZOSL-1 cells produce tumors and metastasis in nude mice, making it a suitable model for evaluating OS lung metastasis.

3.7. Expression of metastasis related genes

In order to further explore mutation characteristics, whole-exon sequencing analysis was performed on ZOSL-1 cells (P20). Results showed that 80,273 SNPS were found in the sample, 98.26% of them were in the dbSNP database and 92.66% were in the 1000 Genomes Project database. There are 1,397 newly discovered SNPs. In overall SNPS, coding area is 9240 synonymous mutations, 9166 missense mutations, there are 40 SNP causes termination codon into the termination codon, 113 SNPs that codon is a termination codon, 26 SNPs that starting codes into the start codon, 138 SNPS in the splice site area change splicing receptors or splice donor (Supplementary Table S2).

To further investigate the metastasis ability of ZOSL-1 cells, we evaluated the expression level of some metastasis related genes. Results showed that GNAS and SCARB1 gene expression was significantly higher than that in hFOB1.19 cells. FAS, NF2 and EZR gene

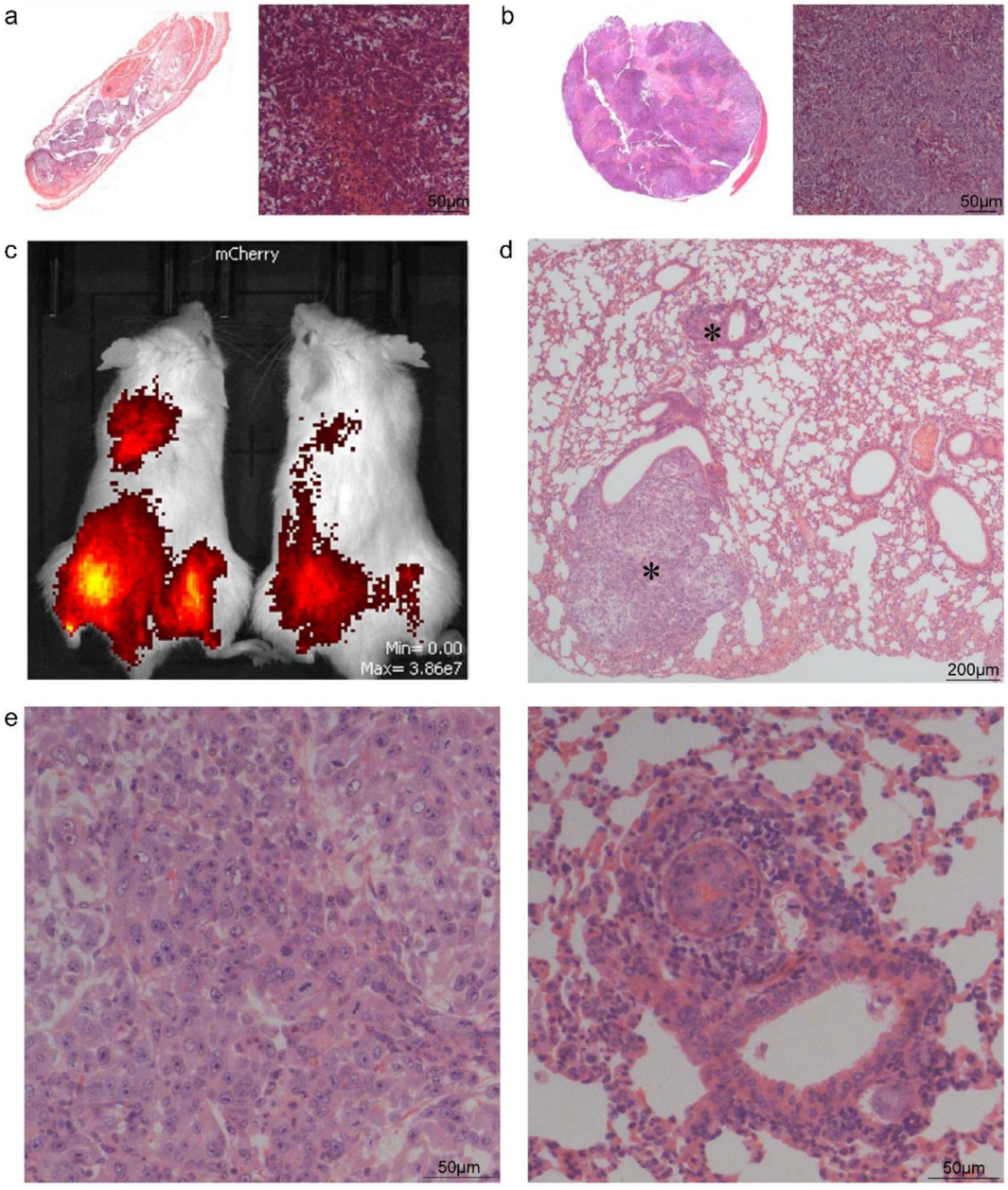

Fig. 5. ZOSL-1 cells had the tumorigenicity and metastatic capacity *in vivo*. a: HE of subcutaneous tumor. b: HE of orthotopic mice model. c: In situ tumor metastasis was detected by *in vivo* imaging. d: HE of lung tissue. E: Enlargements of a tumor in lung tissue.

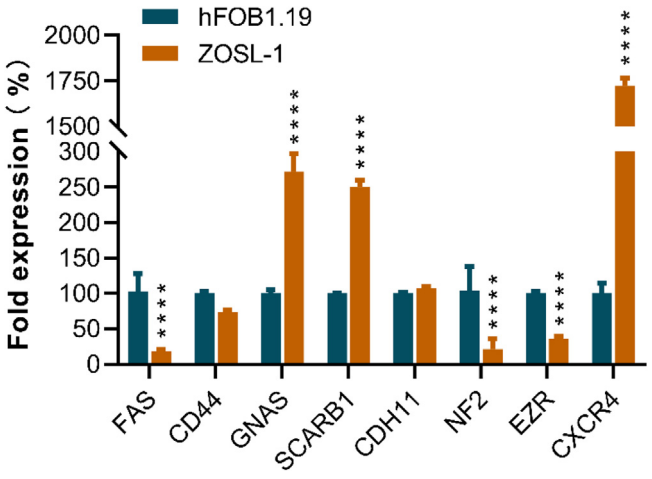

Fig. 6. Comparison of the expression of a part of metastasis-related genes by RT-PCR. FAS, NF2 and EZR significant reduced compared to hFOB1.19. GNAS, SCARB1 and CXCR4 increased in ZOSL-1. No difference of CD44 and CDH11 were found between ZOSL-1 and osteoblast cells. ****: $p < 0.0001$; ***: $p < 0.001$; **: $p < 0.01$, *: $p < 0.05$.

expression was significantly lower than that of hFOB 1.19 cells (Fig. 6). No difference of CD44 and CDH11 were found between ZOSL-1 and osteoblast cells. GNAS, SCARB1 and CXCR4 genes were participated in tumor growth and metastasis, and these genes were up-regulated in ZOSL-1 cells when compared to osteoblast cells. The down-regulate of FAS gene expression level make tumor cells more possible survival in lung tissue, due to the suppression of exogenous apoptotic pathway [13]. NF2 and EZR genes can maintain normal adhesion function and migration function of cell. The remarkably reduction of NF2 and EZR expression in ZOSL-1 cell may promote its migration ability and induce pulmonary metastasis. These results indicated that high metastasis ability of ZOSL-1 may be related to expression changes of these five genes.

4. Discussion

The establishment of OS lung metastasis cells is critical to the study of OS, and the establishment of D17 cells makes it possible to separate and culture OS lung metastasis cells directly [13], but has not been reported in human cell lineage. In our study, ZOSL-1 cells were directly isolated from OS lung metastases. ZOSL-1 cells resulted a new cell line as compared with ATCC or DSMZ human cell line STR profile databases (Supplementary Fig. S3). No contamination by another human cell line and other species was detected. Morphologically, ZOSL-1 cells were polygonal in shape, with large and multiple nucleoli, and abundant organelles. ZOSL-1 cells have potential to proliferate and clonal formation in vitro, and steadily expand to 50 generations. The population doubling time was 39.28 ± 3.04 h, slightly higher than that of HOS (34 h), Zos (33.65 h), Zos-M (31.58 h) and CHOS (36 h) cells [10,12,15]. This phenomenon of steadily proliferated ability means ZOSL-1 cells can be confirmed as a matured OS cell line.

Metastasis is an important factor affecting the prognosis of OS. In studies by Zou *et al.*, OS cells obtained from skip lesions showed stronger metastasis efficiency than that from the primary tumor [12]. Our tissue samples were obtained from metastatic lung tumors after chemotherapy. Of course, it is best to use non-chemotherapy samples, but OS is more aggressive and requires chemotherapy before surgery, so it is difficult to obtain non-chemotherapy samples for research. In 2019, a paper published in the Nature Genetics showed that the ratio of mutations caused by oxaliplatin that affects the known cancer gene sequence was about 0.6/1000, and the ratio was 1.47/1000 in naturally occurring gene mutations [16]. Therefore, the probability of gene mutation caused by chemotherapy is relatively low. Then, we investigated the in vitro and *in vivo* metastatic potential of ZOSL-1 cells. In vitro scratch and transwell assay results showed that ZOSL-1 cells possessed significant migration and invasion properties, compared to hFOB 1.19 (Supplementary Figure S4). In previous reports on cell metastasis, most of the *in vivo* organic metastatic model involved caudal vein injections [15]. However, ZOSL-1 cells can metastasize to the lung in the *in situ* tumor model with a metastasis rate of 100%, as shown by *in vivo* imaging. Generally, ZOSL-1 cells were conducive to establish lung metastasis model and suitable for future research on lung metastasis of OS. In addition, this cell line may help to reveal new prognostic factors for patients with pulmonary metastasis after chemotherapy.

Chromosomal variation has a high incidence in tumors and is closely related to the occurrence and development of tumors. In our study, ZOSL-1 cells were diploid with 48 chromosomes. To further understand ZOSL-1 cells variation, we performed full exon sequencing and detected 80,273 SNPs. We have screened several genes that may play important roles in ZOSL-1 cells function, including FAS, GNAS, SCARB1, CXCR4, NF2 and EZR. In previous reports, the regulated five genes were all related to tumor growth and metastasis mechanisms [17–20]. The high expression of GNAS was associated with poor prognosis of tumors, which has been reported in hepatocellular carcinoma and breast cancer. Through microarray detection of 150 breast cancer tissues, Jin *et al.* assessed the correlation between GNAS expression and clinical prognosis and confirmed that GNAS affected proliferation and EMT process of breast cancer cells through PI3K/AKT/Snail1/E-cadherin signaling pathway. They proposed to use GNAS as a prognostic indicator and a new therapeutic target for breast cancer [17]. A consistent conclusion was reached by Cao *et al.* in hepatocellular carcinoma [21]. SCARB1 as a receptor of high-density lipoprotein-cholesterol, is involved in cholesterol metabolism and has been reported to be closely related to the occurrence and development of prostate cancer, and is a potential target of prostate cancer [18]. In addition, up-regulation of SCARB1 expression is associated with poor prognosis of breast cancer and renal clear cell carcinoma [18–20]. In our study, SCARB1 gene expression was 2.5-fold higher in ZOSL-1 cells, compared with that in hFOB 1.19 cells. The CXCR4 gene was highly related to OS chemo-drug resistant and metastasis, and had been reported in several articles. Jiang et al. reported SDF-1/CXCR4 axis can blunts the response to anti-PD-1 therapy through facilitates myeloid-derived suppressor cells accumulation in OS micro-environment [22]. Ren et al. reported that the SDF-1/CXCR4 axis plays an important role in the metastasis of malignant tumors and the co-expression of CXCR4 and MMP9 was independent predictor of lung metastasis and prognosis [23]. In our study, the ZOSL-1 cells highly expressed CXCR4 and the level of CXCR4 in ZOSL-1 cells was almost eighteen-fold higher than hFOB1.19 cells. This result indicated that the up-regulated CXCR4 gene might be one of the reasons that promoted the powerful metastatic ability of ZOSL-1 cells. In addition, FAS mediates apoptosis, and its ligand is highly expressed in lung tissue. Elizabeth *et al.* showed high expression of FAS effectively inhibit lung metastasis of OS cells [14]. Merlin protein encoded by NF2 inhibits tumor growth and metastasis by inhibiting the FOXM1/β-catenin signaling pathway [24]. The negative expression of EZR is associated with high frequency of breast cancer metastases and decreased metastasis-free survival [25]. In our results, NF2 and EZR decreased significantly than hFOB 1.19. These results suggest that GNAS, FAS, NF2, EZR and SCARB1 are maybe the key genes affecting ZOSL-1 cells metastasis.

In conclusion, we established a new OS cell line named ZOSL-1, which is the first pulmonary metastasis OS cell line. The biological

functions of ZOSL-1 have been verified, and its high metastatic potential supports further model establishment and investigation on OS metastasis mechanisms.

CRediT authorship contribution statement

Zepei Fan: Methodology, Investigation, Writing - original draft, Writing - review & editing. **Guanyu Huang:** Methodology, Validation, Writing - original draft, Writing - review & editing. **Jupeng Zhao:** Methodology, Investigation, Writing - original draft, Writing - review & editing. **Wuguo Li:** Validation, Formal analysis. **Tiao Lin:** Validation, Formal analysis. **Qiao Su:** Resources, Funding acquisition. **Junqiang Yin:** Conceptualization, Resources, Funding acquisition. **Jingnan Shen:** Conceptualization, Resources, Funding acquisition.

Declaration of Competing Interest

The authors declare that they have no known competing financial interests or personal relationships that could have appeared to influence the work reported in this paper.

Acknowledgements

There was no grant support or institutional/corporate affiliation associated with this study.

Funding

This work was supported by the National Natural Science Foundation of China [grant number 81772861]; Natural Science Foundation of Guangdong Province [grant number 2018A030313689]; the Science &Technology Planning Project of Guangzhou City [grant number 201704030008]; the Fundamental Research Funds for the Central Universities [grant number 19ykzd10]; the Science & Technology Planning Project of Guangdong Province [grant numbers 2017A050501015, 2018B030317001, 2019A030317005] and Scientific Research 3 × 3 Project of Sun Yat-Sen University [grant numbers Y70215).

Ethical approval

All applicable international, national, and/or institutional guidelines for the care and use of animals were followed. All procedures performed in studies involving human participants were in accordance with the ethical standards of the institutional and/or national research committee and with the 1964 Helsinki declaration and its later amendments or comparable ethical standards.

Appendix A. Supplementary data

Supplementary data to this article can be found online at https://doi.org/10.1016/j.jbo.2021.100378.

References

[1] A.M. Czarnecka, K. Synoradzki, W. Firlej, E. Bartnik, P. Sobczuk, M. Fiedorowicz, P. Grieb, P. Rutkowski, Molecular biology of osteosarcoma, Cancers 12 (8) (2020) 27.
[2] G. Ottaviani, N. Jaffe, The epidemiology of osteosarcoma, Cancer Treat. Res. 152 (2009) 3–13.
[3] M. Laschi, G. Bernardini, M. Geminiani, L. Ghezzi, L. Amato, D. Braconi, L. Millucci, B. Frediani, A. Spreafico, A. Franchi, D. Campanacci, R. Capanna, A. Santucci, Establishment of four new human primary cell cultures from chemo-Naïve Italian osteosarcoma patients, J. Cell. Physiol. 230 (11) (2015) 2718–2727.
[4] C. Schwartz, R. Gorlick, L. Teot, M. Krailo, Z. Chen, A. Goorin, H. Grier, M. Bernstein, P. Meyers, Multiple drug resistance in osteogenic sarcoma: INT0133 from the Children's Oncology Group, J. Clin. Oncol. Official J. Am. Soc. Clin. Oncol. 25 (15) (2007) 2057–2062.
[5] J.P.a.E. Saksel, Two established in vztro cell lines from human mesenchymal tumours, Int. J. Cancer 2 (1967) 434–447.
[6] M. Rohrmoser, M. Kluge, Y. Yahia, A. Gruber-Eber, M. Maqbool, I. Forné, S. Krebs, H. Blum, A. Greifenberg, M. Geyer, N. Descostes, A. Imhof, J. Andrau, C. Friedel, D. Eick, MIR sequences recruit zinc finger protein ZNF768 to expressed genes, Nucl. Acids Res. 47 (2) (2019) 700–715.
[7] K.-H. Lu, S.-C. Su, C.-W. Lin, Y.-H. Hsieh, Y.-C. Lin, M.-H. Chien, R.J. Reiter, S.-F. Yang, Melatonin attenuates osteosarcoma cell invasion by suppression of C-C motif chemokine ligand 24 through inhibition of the c-Jun N-terminal kinase pathway, J. Pineal Res. 65 (3) (2018) e12507, https://doi.org/10.1111/jpi.2018.65.issue-310.1111/jpi.12507.
[8] A. Shostak, B. Ruppert, N. Ha, P. Bruns, U.H. Toprak, R. Eils, M. Schlesner, A. Diernfellner, M. Brunner, MYC/MIZ1-dependent gene repression inversely coordinates the circadian clock with cell cycle and proliferation, Nat. Commun. 7 (1) (2016), https://doi.org/10.1038/ncomms11807.
[9] J.-Q. Yin, J.-N. Shen, W.-W. Su, J. Wang, G. Huang, S. Jin, Q.-C. Guo, C.-y. Zou, H.-M. Li, F.-B. Li, Bufalin induces apoptosis in human osteosarcoma U-2OS and U-2OS methotrexate300-resistant cell lines, Acta Pharmacol. Sin. 28 (5) (2007) 712–720.
[10] R.M. McAllister, M.B. Gardner, A.E. Greene, C. Bradt, W.W. Nichols, B.H. Landing, Cultivation in vitro of cells derived from a human osteosarcoma, Cancer 27 (2) (1971) 397–402.
[11] H.H. Luu, Q. Kang, J.K. Park, W. Si, Q. Luo, W. Jiang, H. Yin, A.G. Montag, M.A. Simon, T.D. Peabody, R.C. Haydon, C.W. Rinker-Schaeffer, T.-C. He, An orthotopic model of human osteosarcoma growth and spontaneous pulmonary metastasis, Clin. Exp. Metastasis 22 (4) (2005) 319–329.
[12] C.-y. Zou, J. Wang, J.-N. Shen, G. Huang, S. Jin, J.-Q. Yin, Q.-C. Guo, H.-M. Li, L. Luo, M. Zhang, L.-J. Zhang, Establishment and characteristics of two syngeneic human osteosarcoma cell lines from primary tumor and skip metastases, Acta Pharmacol. Sin. 29 (3) (2008) 325–332.z.
[13] J.L. Riggs, R.M. McAllister, E.H. Lennette, Immunofluorescent studies of RD-114 virus replication in cell culture, J. Gen. Virol. 25 (1) (1974) 21–29.
[14] E.A. Lafleur, N.V. Koshkina, J. Stewart, S.-F. Jia, L.L. Worth, X. Duan, E.S. Kleinerman, Increased fas expression reduces the metastatic potential of human osteosarcoma cells, Clin. Cancer Res. 10 (23) (2004) 8114–8119.
[15] Y. Liu, X. Feng, Y. Zhang, H. Jiang, X. Cai, X. Yan, Z. Huang, F. Mo, W. Yang, C. Yang, S. Yang, X. Liu, Establishment and characterization of a novel osteosarcoma cell line: CHOS, J. Orthop. Res. Official Publ. Orthop. Res. Soc. 34 (12) (2016) 2116–2125.
[16] O. Pich, F. Muiños, M.P. Lolkema, N. Steeghs, A. Gonzalez-Perez, N. Lopez-Bigas, The mutational footprints of cancer therapies, Nat. Genet. 51 (12) (2019) 1732–1740.
[17] X. Jin, L. Zhu, Z. Cui, J. Tang, M. Xie, G. Ren, Elevated expression of GNAS promotes breast cancer cell proliferation and migration via the PI3K/AKT/Snail1/E-cadherin axis, Clin. Transl. Oncol. Official Publ. Federation Spanish Oncol. Soc. Natl. Cancer Inst. Mexico 21 (9) (2019) 1207–1219.
[18] J.A. Gordon, J.W. Noble, A. Midha, F. Derakhshan, G. Wang, H.H. Adomat, E.S. Tomlinson Guns, Y.-Y. Lin, S. Ren, C.C. Collins, P.S. Nelson, C. Morrissey, K.M. Wasan, M.E. Cox, Upregulation of scavenger receptor B1 Is required for steroidogenic and nonsteroidogenic cholesterol metabolism in prostate cancer, Cancer Res. 79 (13) (2019) 3320–3331.
[19] G. Xu, N. Lou, Y. Xu, H. Shi, H. Ruan, W. Xiao, L. Liu, H. Xiao, B. Qiu, L. Bao, C. Yuan, K. Chen, H. Yang, X. Zhang, Diagnostic and prognostic value of scavenger receptor class B type 1 in clear cell renal cell carcinoma, Tumour Biol. J. Int. Soc. Oncodevelopmental Biol. Med. 39 (5) (2017) 1–8.
[20] B. Yuan, C. Wu, X. Wang, D. Wang, H. Liu, L. Guo, X. Li, J. Han, H. Feng, High scavenger receptor class B type I expression is related to tumor aggressiveness and poor prognosis in breast cancer, Tumour Biol. J. Int. Soc. Oncodevelopmental Biol. Med. 37 (3) (2016) 3581–3588.
[21] X. Cao, H. Ji, Y. Zhou, X. Lu, J. Shen, Z. Wu, H. Bu, Y. Shi, Elevated expression of Gα in intrahepatic cholangiocarcinoma associates with poor prognosis, Hepatob. Pancreatic Dis. Int. HBPD Int. 16 (6) (2017) 638–644.
[22] K. Jiang, J. Li, J. Zhang, L. Wang, Q. Zhang, J. Ge, Y. Guo, B. Wang, Y.i. Huang, T. Yang, D. Hao, L. Shan, SDF-1/CXCR4 axis facilitates myeloid-derived suppressor cells accumulation in osteosarcoma microenvironment and blunts the response to anti-PD-1 therapy, Int. Immunopharmacol. 75 (2019) 105818, https://doi.org/10.1016/j.intimp.2019.105818.
[23] Z. Ren, S. Liang, J. Yang, X. Han, L. Shan, B. Wang, T. Mu, Y. Zhang, X. Yang, S. Xiong, G. Wang, Coexpression of CXCR4 and MMP9 predicts lung metastasis and poor prognosis in resected osteosarcoma, Tumour Biol. 37 (4) (2016) 5089–5096.
[24] Ming Quan, Jiujie Cui, Tian Xia, Zhiliang Jia, Dacheng Xie, Daoyan Wei, Suyun Huang, Qian Huang, Shaojiang Zheng, K. Xie, Merlin/NF2 suppresses pancreatic tumor growth and metastasis by attenuating the FOXM1-mediated Wnt/β-catenin signaling, Cancer Res. 75(22) (2015) 13.
[25] T.S. Gerashchenko, S.Y. Zolotaryova, A.M. Kiselev, L.A. Tashireva, N.M. Novikov, N.V. Krakhmal, N.V. Cherdyntseva, M.V. Zavyalova, V.M. Perelmuter, E.V. Denisov, The activity of KIF14, mieap, and EZR in a New type of the invasive component, torpedo-like structures, predetermines the metastatic potential of breast cancer, Cancers 12 (7) (2020).